

# MCDS-VSS: Moving Camera Dynamic Scene Video Semantic Segmentation by Filtering with Self-Supervised Geometry and Motion

Angel Villar-Corrales  
villar@ais.uni-bonn.de

Moritz Austermann  
s6mozapp@uni-bonn.de

Sven Behnke  
behnke@cs.uni-bonn.de

Autonomous Intelligent Systems  
University of Bonn  
Friedrich-Hirzebruch-Allee 5  
53115 Bonn, Germany

## Abstract

Autonomous systems, such as self-driving cars, rely on reliable semantic environment perception for decision making. Despite great advances in video semantic segmentation, existing approaches ignore important inductive biases and lack structured and interpretable internal representations. In this work, we propose *MCDS-VSS*, a structured filter model that learns in a self-supervised manner to estimate scene geometry and ego-motion of the camera, while also estimating the motion of external objects. Our model leverages these representations to improve the temporal consistency of semantic segmentation without sacrificing segmentation accuracy. *MCDS-VSS* follows a prediction-fusion approach in which scene geometry and camera motion are first used to compensate for ego-motion, then residual flow is used to compensate motion of dynamic objects, and finally the predicted scene features are fused with the current features to obtain a temporally consistent scene segmentation. Our model parses automotive scenes into multiple decoupled interpretable representations such as scene geometry, ego-motion, and object motion. Quantitative evaluation shows that *MCDS-VSS* achieves superior temporal consistency on video sequences while retaining competitive segmentation performance. Animations and code to reproduce our results can be found in our [project website](#).

## 1 Introduction

Video semantic segmentation (VSS) is the task of assigning a categorical label to each pixel in every frame of a video sequence [6]. This task is highly relevant in the field of robotics, where understanding and interpreting scenes from video is crucial for many applications, e.g. autonomous driving [4] or indoor service tasks [9]. Thanks to the availability of high-quality image datasets, semantic segmentation of automotive scenarios has recently seen tremendous progress [6, 2, 9]. However, obtaining temporally consistent segmentation of video sequences still remains a challenge due to the lack of large-scale annotated video datasets and the lack of suitable inductive biases for video processing.

To address these limitations, existing VSS models enforce temporal continuity by propagating features across multiple frames through the use of unstructured recurrent networks [8, 42], optical flow models [9, 10], or transformers [28, 51]; thus exploiting temporal correlations in the video sequences in a data-driven manner.

However, these models ignore specific properties from the target domain, which could potentially be incorporated into the model architecture in order to improve its performance and generalization capabilities. For instance, in the automotive domain, the observations taken from a moving vehicle can be decomposed into *static background features*, which move only due to the ego-motion of the vehicle, and *dynamic object features* that correspond to moving objects. Incorporating such motion and geometric inductive biases into the network architecture can lead to models producing a more temporally consistent interpretation of the scene, outperforming models that attempt to learn these properties solely from data.

To test this hypothesis, we propose *MCDS-VSS*, a structured recurrent model that explicitly incorporates geometry and motion inductive biases from the *moving camera dynamic scene* (MCDS) domain in order to improve the temporal consistency of a segmentation network. MCDS-VSS follows a prediction-fusion approach in which ego-motion is compensated by projecting scene features into the current time-step using estimated scene geometry and estimated camera motion. Estimated residual flow is then used to compensate for object motion. Finally, the predicted features are fused with the features extracted from the current frame to obtain a temporally consistent semantic segmentation of the scene.

Through self-supervised learning (SSL), MCDS-VSS learns to estimate scene geometry and ego-motion. It also estimates motion of additional objects (e.g. pedestrians or vehicles), and hard-wires our knowledge from the MCDS domain to project the previous scene features into the current time-step using these representations. The structured design of our filter allows us to factorize the perceived complex changes in the scene into simpler factors of variation; thus easing the modeling of temporal information.

Our experiments show that MCDS-VSS improves the temporal consistency of a segmentation model without compromising its segmentation performance, outperforming VSS baselines which ignore moving camera dynamic scene inductive biases, and performing comparably to state-of-the-art VSS models. Furthermore, MCDS-VSS parses an automotive scene into interpretable internal representations, such as depth, camera motion, and object flow.

In summary, our contributions are as follows:

- We propose MCDS-VSS, a structured recurrent filter that improves the temporal consistency of a segmentation model without sacrificing segmentation performance.
- MCDS-VSS learns depth and ego-motion in a self-supervised way, and uses these representations together with estimated object motion to propagate scene features.
- Our model outperforms existing VSS baselines on Cityscapes—achieving superior temporal consistency and parsing the scene into human-interpretable representations.

## 2 Related Work

**Video Semantic Segmentation:** VSS methods are often divided into two distinct categories. The first class aims to reduce the computational cost and improve the efficiency of segmentation models, instead of naively encoding and interpreting every single input frame. Several methods improve the efficiency by propagating and reusing features extracted from selected key frames [22, 53]; whereas other approaches achieve efficiency by

employing lightweight neural network blocks [85, 40] or by distilling the information from large teacher models to smaller models [80]. The second category, to which our proposed method belongs, aims to improve the semantic segmentation performance and temporal consistency by exploiting the temporal continuity of video streams. Some methods exploit temporal dependencies between video frames and improve the consistency of the predicted segmentation maps by combining image segmentation models with recurrent neural networks (RNNs) [66, 40, 42, 48] or with attention-based modules [26, 28, 44, 45, 51]. Another family of works use an optical flow module to compute the feature correspondence between consecutive frames, and then use this flow for predictive feature learning [0, 9, 20, 80, 47, 54, 53].

Our method belongs to the latter category. However, unlike aforementioned approaches, MCDS-VSS incorporates assumptions from the domain of moving cameras and dynamic scenes into the model design, computing interpretable intermediate representations, which lead to more temporally consistent video segmentation results.

**Improving Segmentation via Depth & Camera Motion Estimation:** Self-supervised depth estimation (SSDE) aims to learn the scene geometry from unlabeled monocular videos, without any recorded depth information. This is often achieved by training a neural network to jointly predict the scene depth and camera ego-motion between two video frames, synthesizing the second frame from the first using differentiable warping, and minimizing a photometric loss function [0, 11, 14, 50, 61].

The interplay between semantic segmentation and SSDE has been studied for various tasks, including depth estimation [56], domain adaptation [15, 25, 53], and semi-supervised learning [18, 62]. These models exploit SSDE as an additional source of supervision, helping segmentation models learn high-level semantic features, especially when few labeled samples are available.

Several works have investigated the use of depth and motion for semantic segmentation in videos. Approaches like [0, 6, 41, 62] segment dynamic scenes by jointly processing video frames with depth information captured by LiDAR scanners; whereas methods like [0, 24, 61, 58] use depth and pose information to enforce consistency between segmentation maps from multiple viewpoints. Recently, depth-aware panoptic segmentation (PS) models [54, 57, 59] aim to jointly solve the tasks of PS and depth estimation by extending a segmentation model with a depth decoder and conditioning its prediction using instance-masks.

The method most similar to ours is Wagner *et al.* [49], which leverages depth and camera motion learned in a supervised manner to improve the performance of a segmentation model on video sequences. However, this method has several limitations, including not modeling moving objects and requiring ground truth depth and poses, thus limiting its applicability. In contrast, MCDS-VSS addresses the limitations, being able to process challenging dynamic scenes with moving cameras, even in the absence of depth and camera poses.

### 3 MCDS-VSS Structured Filtering Method

We propose MCDS-VSS, illustrated in Fig. 1, a structured filter that improves the temporal consistency of a semantic segmentation model on moving camera dynamic scene scenarios. MCDS-VSS learns in a self-supervised way to estimate geometry and motion representations, i.e., scene depth and camera ego-motion. It also estimates the motion of other agents in the scene, and uses these human-interpretable representations to propagate abstract scene features over time, thus improving its segmentation performance and temporal consistency.

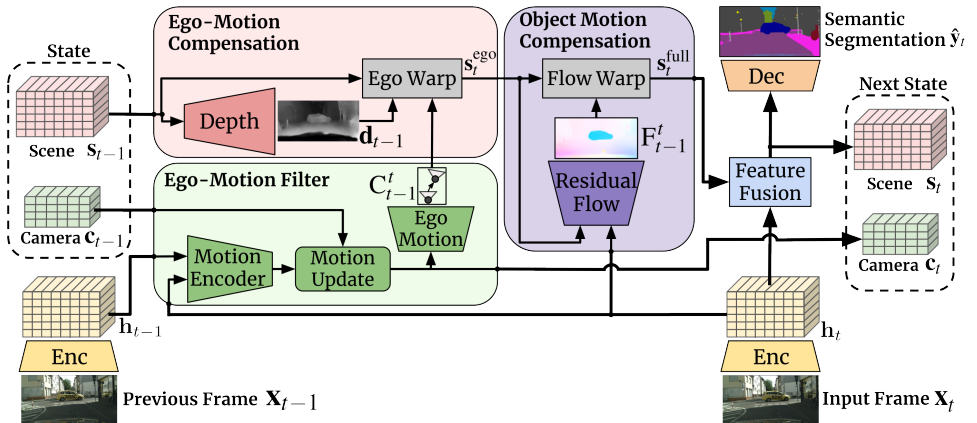


Figure 1: MCDS-VSS structured filter. Scene depth  $\mathbf{d}_{t-1}$ , ego-motion  $\mathbf{C}_{t-1}^t$ , and object-motion  $\mathbf{F}_{t-1}^t$  are used to project scene features  $\mathbf{s}_{t-1}$  to the current time  $t$ , where they are fused with current image features  $\mathbf{h}_t$  to obtain a temporally consistent semantic segmentation  $\hat{\mathbf{y}}_t$ .

MCDS-VSS is composed of an image encoder  $\mathcal{E}_x$ , a structured filter, and a segmentation decoder  $\mathcal{D}_y$ . It receives as input a sequence of RGB frames  $\mathcal{X} = \{\mathbf{x}_1, \dots, \mathbf{x}_T\}$  and encodes them into feature maps  $\{\mathbf{h}_1, \dots, \mathbf{h}_T\}$ , which are then recursively processed to integrate temporal information, and decoded into semantic segmentation maps  $\mathcal{Y} = \{\hat{\mathbf{y}}_1, \dots, \hat{\mathbf{y}}_T\}$ .

### 3.1 Learning of Geometry & Motion

MCDS-VSS learns in a self-supervised manner to estimate scene geometry and camera motion, which are then used to improve the temporal consistency of a segmentation model. Fig. 2 illustrates our two-step self-supervised approach for learning the scene geometry with camera motion and for distillation of object dynamics.

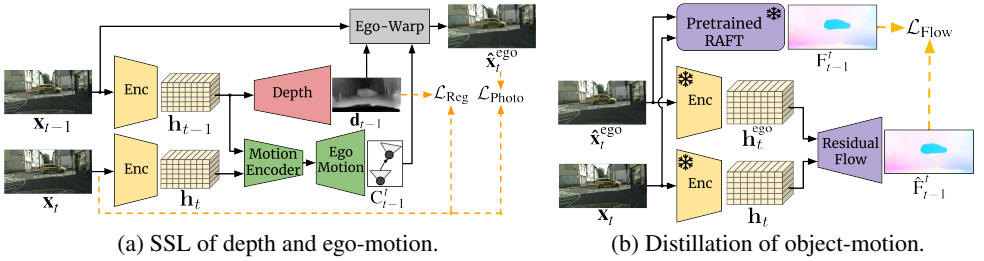
**Scene Geometry and Ego-Motion:** We train our model to predict the monocular depth and camera pose transformation of the vehicle in a self-supervised manner by solving a novel view-synthesis pretext task in which a target image  $\mathbf{x}_t$  is rendered from a source image  $\mathbf{x}_{t-1}$  by modeling the static scene features that change due to the ego-motion [13, 51].

To predict the scene geometry, MCDS-VSS incorporates a *depth decoder*  $\mathcal{D}_d$  that outputs the depth  $\mathbf{d}_t$  and inverse depth  $\mathbf{d}_t^{\leftarrow 1}$  of the scene given the input feature maps  $\mathbf{h}_t$ ; whereas to compute the camera motion between two images we employ a *motion encoder*  $\mathcal{E}_m$  that computes motion features between two sets of feature maps, and an *ego-motion decoder*  $\mathcal{D}_c$ , which predicts the camera transformation between two time steps  $\mathbf{C}_{t-1}^t$ , parameterized as a 6-dim. vector containing the translation and Euler angles of the camera transformation matrix. We then render the ego-warped image  $\hat{\mathbf{x}}_t^{\text{ego}}$  using the estimated depth and ego-motion:

$$\hat{\mathbf{x}}_t^{\text{ego}} = \mathcal{F}_{\text{fwd}}(\mathbf{x}_{t-1}, \mathbf{d}_{t-1}, \mathbf{C}_{t-1}^t, K), \quad (1)$$

where  $K \in \mathbb{R}^{3,3}$  are the camera intrinsic parameters, and  $\mathcal{F}_{\text{fwd}}$  is the forward rendering function proposed in [27]. If the depth and ego-motion estimates are accurate, the resulting warped images should match the target images except for occluded regions and moving objects. Therefore, as illustrated in Fig. 2a, we train the modules for self-supervised depth and

<sup>1</sup>With slight abuse of notation, we denote the  $\mathbf{d}_t^{\leftarrow}$  as *disparities*.



(a) SSL of depth and ego-motion.

(b) Distillation of object-motion.

Figure 2: Learning geometry and motion. a) We learn the depth  $\mathbf{d}_{t-1}$  and ego-motion  $C_{t-1}^e$  given two video frames by enforcing a photometric loss between warped and target frame  $\mathcal{L}_{\text{Photo}}$  and a depth regularization  $\mathcal{L}_{\text{Reg}}$ . b) Given an ego-warped image, we train a flow decoder to model the dynamics of moving objects by distilling a pretrained RAFT model.

ego-motion estimation by optimizing the following loss function:

$$\mathcal{L}_{\text{Depth}} = \mathcal{L}_{\text{Photo}}(\hat{\mathbf{x}}_t^{\text{ego}}, \mathbf{x}_t) + \lambda_{\text{Reg}} \cdot \mathcal{L}_{\text{Reg}}(\mathbf{d}_{t-1}^{\square}), \quad (2)$$

$$\mathcal{L}_{\text{Photo}} = \frac{\alpha}{2}(1 - \text{SSIM}(\hat{\mathbf{x}}_t^{\text{ego}}, \mathbf{x}_t)) + (1 - \alpha)\|\hat{\mathbf{x}}_t^{\text{ego}} - \mathbf{x}_t\|, \quad (3)$$

$$\mathcal{L}_{\text{Reg}} = |\partial_x \tilde{\mathbf{d}}_t^{\square}| e^{-|\partial_x \mathbf{x}_t|} + |\partial_y \tilde{\mathbf{d}}_t^{\square}| e^{-|\partial_y \mathbf{x}_t|}, \quad (4)$$

where  $\partial_x$  and  $\partial_y$  are the spatial gradients in the  $x$ - and  $y$ -directions, SSIM is the structural similarity index, and  $\tilde{\mathbf{d}}^{\square}$  is the normalized disparity map.  $\mathcal{L}_{\text{Photo}}$  is a photometric loss that measures the difference between the ego-warped and target images, and  $\mathcal{L}_{\text{Reg}}$  is an edge-aware smoothing regularization [10] that encourages the normalized disparity maps to be locally smooth, except on the image edges. To mitigate the effect of disocclusions and moving objects during training, we use the auto-masking and per-pixel minimum processing steps proposed in [10].

**Object Motion:** Assuming static scenes as well as accurate depth and ego-motion estimates, the predicted ego-warped images  $\hat{\mathbf{x}}_t^{\text{ego}}$  are identical, up to occluded regions, to the target images  $\mathbf{x}_t$ . Hence, we make the assumption that any major differences between such frames must be explained by external moving objects (e.g. driving cars or pedestrians).

As illustrated in Fig. 2b, we estimate the residual optical flow  $\hat{\mathbf{F}}_{t-1}^t$  between the ego-warped and target images, which parameterizes the dynamics of moving objects, by training an *residual flow decoder*  $\mathcal{R}_f$  while keeping all other modules frozen.  $\mathcal{R}_f$  is trained to match the optical flow predictions of the large state-of-the-art optical flow model RAFT [46]:

$$\mathcal{L}_{\text{Flow}} = \|\hat{\mathbf{F}}_{t-1}^t - \mathbf{F}_{t-1}^t\|_1. \quad (5)$$

## 3.2 Structured Filter

The modules and representations described in Section 3.1 form the core of the MCDS-VSS structured filter, which is depicted in Fig. 1. It propagates information over time using two different filter states, namely a *scene state*  $\mathbf{s}$  that encodes the scene contents and geometry and a *camera state*  $\mathbf{c}$ , which encodes the ego-motion of the vehicle.

It consists of six components: ego-motion filter, depth estimation, ego-motion compensation, residual flow estimation, object motion compensation, and feature fusion.

**Ego-Motion Filter:** The ego-motion filter extends the motion encoder and camera predictor modules in order to aggregate motion information over time and enforce the prediction of

temporally consistent ego-motion. The temporal integration is achieved via a *motion update* module, which is implemented as a ConvGRU [9] recurrent layer that jointly processes the motion features and previous camera state  $\mathbf{c}_{t-1}$  and outputs an updated camera state  $\mathbf{c}_t$  from which the ego-motion can be then predicted:

$$\mathbf{c}_t = \text{ConvGRU}(\mathcal{E}_m(\mathbf{h}_t, \mathbf{h}_{t-1}), \mathbf{c}_{t-1}), \quad \mathbf{C}_{t-1}^t = \mathcal{D}_c(\mathbf{c}_t). \quad (6)$$

**Depth Estimation and Ego-Motion Compensation:** Given the past scene state  $\mathbf{s}_{t-1}$ , the *depth decoder*  $\mathcal{D}_d$  computes the depth map  $\mathbf{d}_{t-1}$ . This scene geometry and the ego-motion  $\mathbf{C}_{t-1}^t$  are used as in Eq. (1) to project  $\mathbf{s}_{t-1}$  to time  $t$ . The resulting ego-warped scene state  $\mathbf{s}_t^{\text{ego}}$  encodes scene contents and geometry after compensation for ego-motion.

**Object-Motion Compensation:** This module models dynamic objects in the scene, such as pedestrians or vehicles, and updates the scene state to compensate for the motion of such objects. We jointly process the ego-warped scene state  $\mathbf{s}_t^{\text{ego}}$  and the current image features  $\mathbf{h}_t$  with the residual flow decoder  $\mathcal{R}_f$  in order to compute the residual flow  $\hat{\mathbf{F}}_{t-1}^t$ , which represents the pixel displacement of moving objects between consecutive time steps. The ego-warped features  $\mathbf{s}_t^{\text{ego}}$  are then projected into the current time-step by applying the displacement encoded in the residual flow map, followed by bilinear interpolation to obtain valid coordinate values. The resulting features  $\mathbf{s}_t^{\text{full}}$  not only incorporate the motion of dynamic objects in the scene, but can also correct alignment errors between  $\mathbf{s}_t^{\text{ego}}$  and  $\mathbf{h}_t$  that might occur due to inaccurate depth or ego-motion estimates.

**Feature Fusion:** While the previous modules propagate scene features over time, the *feature fusion* module allows MCDS-VSS to combine the projected scene features  $\mathbf{s}_t^{\text{full}}$  with the observed encoded features  $\mathbf{h}_t$ . This fusion operation is performed by an update gate mask  $\mathbf{u} \in [0, 1]$ , which determines in a data-driven manner for each feature map and spatial location whether one can rely on the current features  $\mathbf{h}_t$  or on prior knowledge propagated through the filter  $\mathbf{s}_t^{\text{full}}$ . The resulting fused scene features  $\mathbf{s}_t$  are part of the next state of the MCDS-VSS filter. More formally, this process can be described as:

$$\mathbf{u} = \sigma(\text{Conv}_s(\mathbf{s}_t^{\text{full}}) + \text{Conv}_h(\mathbf{h}_t) + b), \quad (7)$$

$$\mathbf{s}_t = \mathbf{u} \odot \mathbf{s}_t^{\text{full}} + (1 - \mathbf{u}) \odot \mathbf{h}_t, \quad (8)$$

where  $\text{Conv}_s$  and  $\text{Conv}_h$  are convolution blocks,  $b$  a learned bias, and  $\sigma$  the sigmoid function.

### 3.3 Model Training

MCDS-VSS consists of multiple components addressing different subtasks: depth estimation, ego-motion estimation, ego-motion compensation, object motion estimation, object motion compensation, and feature fusion. Naively training such a model in an end-to-end manner with a video segmentation objective can result in bad local optima, where the model does not learn interpretable representations (e.g. depth or object flow).

To ease the training process, we propose a multi-stage approach in which we first train the encoder and decoder modules using image pairs or triplets, and then integrate and train the filter modules using sequences of six frames in order to improve segmentation performance and temporal consistency while retaining interpretable representations.

MCDS-VSS undergoes a four-stage training process, outlined in Table 1. Initially, as detailed in Section 3.1, MCDS-VSS encoder and decoder modules are jointly trained for self-supervised learning of geometry and ego-motion, as well as for semantic segmentation

Table 1: Training stages and hyper-parameters.

Stage	Training Goal	Loss Function	LR	# Imgs
1	Segmentation & SSL Geometry	$\mathcal{L}_{\text{Seg}} + \lambda_{\text{D}} \cdot \mathcal{L}_{\text{Depth}}$ (2)	$2 \cdot 10^{-4}$	3
2	Distillation of Object Motion	$\mathcal{L}_{\text{Flow}}$ (5)	$1 \cdot 10^{-4}$	2
3	Ego-Motion Filter	$\mathcal{L}_{\text{Ego}}$ (9)	$8 \cdot 10^{-5}$	6
4	Temporal Integration	$\mathcal{L}_{\text{Seg}} + \lambda_{\text{TC}} \cdot \mathcal{L}_{\text{TC}}$ (10)	$8 \cdot 10^{-5}$	6

by minimizing a combination of cross entropy  $\mathcal{L}_{\text{Seg}}$  and SSL geometry  $\mathcal{L}_{\text{Depth}}$  losses. Following [13], we use image triplets  $(\mathbf{x}_{t-\tau}, \mathbf{x}_t, \mathbf{x}_{t+\tau})$ , with  $\mathbf{x}_t$  being the target. Subsequently, we train the residual flow decoder as described in Section 3.1 while keeping the remaining modules frozen. In the third stage, with the goal of improving the temporal continuity of the predicted ego-motion, we train the ego-motion filter and compensation by minimizing the loss function:

$$\mathcal{L}_{\text{Ego}} = \frac{1}{T} \sum_{t=1}^T \mathcal{L}_{\text{Photo}}(\hat{\mathbf{x}}_t^{\text{ego}}, \mathbf{x}_t), \quad (9)$$

which enforces the model to compute accurate camera motion estimates in order to align the ego-warped state with the current observations. Finally, we jointly train the fusion module and fine-tune the segmentation decoder by minimizing the following loss function:

$$\mathcal{L} = \frac{1}{T} \sum_{t=1}^T \mathcal{L}_{\text{Seg}}(\hat{\mathbf{y}}_t, \mathbf{y}_t) + \lambda_{\text{TC}} \cdot \mathcal{L}_{\text{TC}}(\tilde{\mathbf{y}}_t, \hat{\mathbf{y}}_t), \quad (10)$$

where  $\mathcal{L}_{\text{Seg}}$  is the cross entropy loss function and  $\mathcal{L}_{\text{TC}}$  is a temporal consistency regularizer that enforces the segmentation  $\tilde{\mathbf{y}}_t$  computed by decoding  $\mathbf{s}_t^{\text{full}}$  to be close to the actual predicted segmentation maps  $\hat{\mathbf{y}}_t$ .

## 4 Experimental Evaluation

### 4.1 Experiment Setup

**Dataset:** We evaluate MCDS-VSS on the Cityscapes [8] dataset, which contains 5,000 automotive video sequences, each containing 30 images of size  $1024 \times 2048$ , recorded in 50 German cities, where only the 20th frame is annotated. This dataset is a good benchmark for our model, since it contains real-world dynamic scenes recorded from a moving vehicle. We augment the data using color jittering, mirroring, and random cropping.

**Evaluation Metrics:** We evaluate the segmentation performance and temporal consistency of our model. The performance is evaluated using the mean Intersection-over-Union (mIoU). Following [30], we measure the temporal consistency (TC) of our predicted segmentation maps by computing the mean flow warping error between every two neighboring frames. Our results are computed using single-scale testing on the full image resolution.

**Implementation Details:** We train two MCDS-VSS variants using distinct image encoder and segmentation decoder architectures. Namely, a small variant based on DeepLabV3+ [9] with ResNet18 [17] backbone, and a larger variant based on HRNetV2 [52]. The depth and pose decoders closely follow [13], which output inverse depth maps and a 6-dimensional vector containing the camera translation and Euler angles, respectively. Finally, our residual flow decoder is a lightweight version of RAFT [46], for which, to integrate into our filter, we

Table 2: Comparison of segmentation models on the Cityscapes validation set using different backbones. Best two results are highlighted in boldface and underlined, respectively.

Model	Backbone	Cityscapes	
		mIoU $\uparrow$	TC $\uparrow$
DeepLabV3+ [10]	ResNet18	75.2	69.8
Accel [12]	ResNet18	72.1	70.3
SKD [14]	ResNet18	74.5	68.2
ETC [60]	PSPNet18	73.1	70.6
ETC [60]	MobileNetV2	73.9	69.9
TCNet [47]	ResNet18	62.2	72.1
TDNet [49]	BiSeNet18	75.0	70.2
TDNet [49]	PSPNet18	<u>76.8</u>	70.4
STT [28]	BiSeNet18	75.8	71.4
STT [28]	ResNet18	<b>77.3</b>	<u>73.0</u>
MCDS-VSS (ours)	ResNet18	75.1	<b>74.5</b>

Model	Backbone	Cityscapes	
		mIoU $\uparrow$	TC $\uparrow$
HRNetV2 [62]	HRNetV2	76.3	70.6
Accel [12]	ResNet50	74.2	-
ETC [60]	HRNetV2	76.4	70.1
ETC [60]	ResNet50	<b>77.9</b>	72.3
AuxAdapt [64]	HRNetV2	76.6	<b>75.3</b>
PC [63]	HRNetV2	76.4	71.2
TCNet [47]	HRNetV2	72.7	<u>74.7</u>
STT [28]	BiSeNet34	<u>77.3</u>	72.0
MCDS-VSS (ours)	HRNetV2	77.1	<b>75.3</b>

replace the context and feature encoders with a single convolutional block. We emphasize that MCDS-VSS is architecture-agnostic and could be implemented with different model designs. Further implementation details are provided in Appendix B.

## 4.2 Comparison with Existing Methods

In Table 2, we quantitatively compare MCDS-VSS with several existing image and video segmentation models using small (left) and larger (right) backbones. For both variants, MCDS-VSS achieves the highest temporal consistency among all compared methods, while retaining a competitive segmentation performance. Furthermore, in contrast to other approaches aiming to improve the TC of a segmentation model, e.g. TCNet [47], MCDS-VSS does not sacrifice segmentation performance in order to improve the temporal consistency, outperforming multiple VSS models for both backbone variants.

In Fig. 3, we show a qualitative result comparing MCDS-VSS with an HRNetV2 baseline. Our method achieves more accurate and temporally consistent segmentations compared to HRNet, correctly segmenting the traffic signs and reducing the amount of flickering between frames. Furthermore, we show MCDS-VSS interpretable intermediate representations, such as the depth of the scene and the residual flow, which encodes the movement of the pedestrians in the scene, as well as some corrections for other objects, such as the hood of the ego-vehicle. Further visualizations can be found in Appendix D.

## 4.3 Ablation Study

To understand the effectiveness of MCDS-VSS, we ablate our filter design and measure the contribution of different steps in our training process.

**Filter Design:** Given the same DeepLabV3+ model trained with the SSL procedure described in Section 3.1, we compare MCDS-VSS with different filter designs, including unstructured RNNs (ConvGRU) [66, 42], optical-flow based filters [10] (flow-only), and a MCDS-VSS variant modeling only the static scene features (geom-only) [49]. The results, reported in Table 3, show that MCDS-VSS, which decouples the modeling of static and dynamic scene features, achieves the best segmentation performance and temporal consistency.

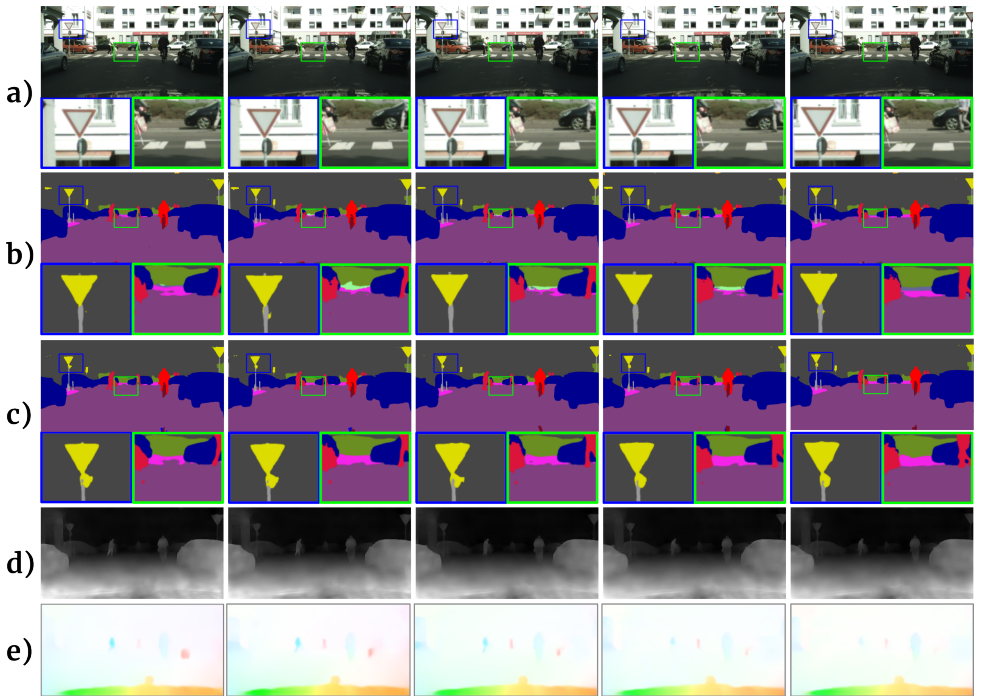


Figure 3: Qualitative evaluation. **a)** Input frames, **b)** HRNetV2, **c)** MCDS-VSS (ours), **d)** Estimated scene depth, **e)** Estimated residual flow. We highlight areas of the segmentation masks where MCDS-VSS obtains visibly more accurate and consistent segmentations.

Table 3: Comparison of various filter designs. We highlight the diff. to baseline.

Model	Results	
	mIoU $\uparrow$	TC $\uparrow$
ResNet18 + SSL	74.76	70.73
+ ConvGRU [10]	73.37 (-1.39)	69.64 (-1.09)
+ Flow-Only [10]	74.95 (+0.19)	73.19 (+2.46)
+ Geom-Only [19]	74.90 (+0.14)	73.80 (+3.07)
+ MCDS-VSS	<b>75.07 (+0.31)</b>	<b>74.53 (+3.80)</b>

Table 4: Effect of SSL geometry & motion and MCDS-VSS. We highlight the diff. to baseline.

Model	Results	
	mIoU $\uparrow$	TC $\uparrow$
ResNet18	75.17	69.89
+ SSL Geom. & Motion	74.76 (-0.44)	70.73 (+0.91)
+ MCDS-VSS	<b>75.07 (-0.10)</b>	<b>74.53 (+4.64)</b>
HRNetV2	76.32	70.58
+ SSL Geom. & Motion	76.45 (+0.13)	71.65 (+1.07)
+ MCDS-VSS	<b>77.14 (+0.82)</b>	<b>75.34 (+4.76)</b>

**Model Ablation:** In Table 4 we measure the effect that our SSL training and MCDS-VSS filter have on the segmentation performance and temporal consistency. For two different segmentation models, i.e. DeepLabV3+ and HRNetV2, we compare the results after each training stage with those of the model trained for image segmentation only. First, we note that SSL training improves the temporal consistency without significantly compromising the segmentation performance. We argue that jointly learning SSL depth and motion with semantic segmentation allows the model to encode the input frames into more robust geometry-aware representations. Finally, the MCDS-VSS filter significantly improves the temporal consistency (>4.6% w.r.t base model), while almost matching the segmentation performance of the base DeepLabV3+ model, and even outperforming HRNetV2.

## 5 Conclusion

We proposed MCDS-VSS, a structured recurrent model for VSS, which learns in a self-supervised manner to estimate scene geometry and camera ego-motion. It also estimates the motion of external objects and leverages these representations to improve the temporal consistency of a semantic segmentation model without sacrificing segmentation performance. MCDS-VSS follows a prediction-fusion approach in which scene geometry and camera motion are first used to compensate for ego-motion, then residual flow is used to compensate the motion of dynamic objects, and finally the projected features are fused with the current observations. In our experiments, we showed that MCDS-VSS outperforms multiple VSS baselines on Cityscapes—achieving superior temporal consistency and parsing the scene into human-interpretable representations.

## Acknowledgments

This work was funded by grant BE 2556/16-2 (Research Unit FOR 2535 Anticipating Human Behavior) of the German Research Foundation (DFG).

## References

- [1] Ali Athar, Enxu Li, Sergio Casas, and Raquel Urtasun. 4D-Former: Multimodal 4D panoptic segmentation. In *Conference on Robot Learning (CoRL)*, pages 2151–2164, 2023.
- [2] Razieh Kaviani Baghbaderani, Yuanxin Li, Shuangquan Wang, and Hairong Qi. Temporally-consistent video semantic segmentation with bidirectional occlusion-guided feature propagation. In *IEEE/CVF Winter Conference on Applications of Computer Vision (WACV)*, pages 685–695, 2024.
- [3] Nicolas Ballas, Li Yao, Chris Pal, and Aaron Courville. Delving deeper into convolutional networks for learning video representations. *International Conference on Learning Representations (ICLR)*, 2016.
- [4] Jia-Wang Bian, Huangying Zhan, Naiyan Wang, Zhichao Li, Le Zhang, Chunhua Shen, Ming-Ming Cheng, and Ian Reid. Unsupervised scale-consistent depth learning from video. *International Journal of Computer Vision (IJCV)*, 129(9):2548–2564, 2021.
- [5] Helin Cao and Sven Behnke. SLCF-Net: Sequential LiDAR-Camera Fusion for Semantic Scene Completion using a 3D Recurrent U-Net. In *IEEE International Conference on Robotics and Automation (ICRA)*, 2024.
- [6] Liang-Chieh Chen, Yukun Zhu, George Papandreou, Florian Schroff, and Hartwig Adam. Encoder-decoder with atrous separable convolution for semantic image segmentation. In *European Conference on Computer Vision (ECCV)*, pages 801–818, 2018.
- [7] Lin-Zhuo Chen, Zheng Lin, Ziqin Wang, Yong-Liang Yang, and Ming-Ming Cheng. Spatial information guided convolution for real-time RGBD semantic segmentation. *IEEE Transactions on Image Processing*, 30:2313–2324, 2021.
- [8] Marius Cordts, Mohamed Omran, Sebastian Ramos, Timo Rehfeld, Markus Enzweiler, Rodrigo Benenson, Uwe Franke, Stefan Roth, and Bernt Schiele. The Cityscapes dataset for semantic urban scene understanding. In *IEEE/CVF Conference on Computer Vision and Pattern Recognition (CVPR)*, pages 3213–3223, 2016.

- [9] Mingyu Ding, Zhe Wang, Bolei Zhou, Jianping Shi, Zhiwu Lu, and Ping Luo. Every frame counts: Joint learning of video segmentation and optical flow. In *Conference on Artificial Intelligence (AAAI)*, volume 34, pages 10713–10720, 2020.
- [10] Raghudeep Gadde, Varun Jampani, and Peter V Gehler. Semantic video CNNs through representation warping. In *IEEE International Conference on Computer Vision (ICCV)*, 2017.
- [11] Ravi Garg, Vijay Kumar Bg, Gustavo Carneiro, and Ian Reid. Unsupervised CNN for single view depth estimation: Geometry to the rescue. In *European Conference on Computer Vision (ECCV)*, pages 740–756, 2016.
- [12] Clément Godard, Oisín Mac Aodha, and Gabriel J Brostow. Unsupervised monocular depth estimation with left-right consistency. In *IEEE/CVF Conference on Computer Vision and Pattern Recognition (CVPR)*, pages 270–279, 2017.
- [13] Clément Godard, Oisín Mac Aodha, Michael Firman, and Gabriel J Brostow. Digging into self-supervised monocular depth estimation. In *IEEE/CVF International Conference on Computer Vision (ICCV)*, pages 3828–3838, 2019.
- [14] Ariel Gordon, Hanhan Li, Rico Jonschkowski, and Anelia Angelova. Depth from videos in the wild: Unsupervised monocular depth learning from unknown cameras. In *IEEE/CVF International Conference on Computer Vision (ICCV)*, pages 8977–8986, 2019.
- [15] Vitor Guizilini, Jie Li, Rares Ambrus, and Adrien Gaidon. Geometric unsupervised domain adaptation for semantic segmentation. In *IEEE/CVF International Conference on Computer Vision (ICCV)*, pages 8537–8547, 2021.
- [16] Kaiming He, Xiangyu Zhang, Shaoqing Ren, and Jian Sun. Deep residual learning for image recognition. In *IEEE/CVF Conference on Computer Vision and Pattern Recognition (CVPR)*, pages 770–778, 2016.
- [17] Andrew Howard, Mark Sandler, Grace Chu, Liang-Chieh Chen, Bo Chen, Mingxing Tan, Weijun Wang, Yukun Zhu, Ruoming Pang, Vijay Vasudevan, et al. Searching for MobileNetV3. In *IEEE/CVF International Conference on Computer Vision (CVPR)*, pages 1314–1324, 2019.
- [18] Lukas Hoyer, Dengxin Dai, Yuhua Chen, Adrian Koring, Suman Saha, and Luc Van Gool. Three ways to improve semantic segmentation with self-supervised depth estimation. In *IEEE/CVF Conference on Computer Vision and Pattern Recognition (CVPR)*, pages 11130–11140, 2021.
- [19] Ping Hu, Fabian Caba, Oliver Wang, Zhe Lin, Stan Sclaroff, and Federico Perazzi. Temporally distributed networks for fast video semantic segmentation. In *IEEE/CVF Conference on Computer Vision and Pattern Recognition (CVPR)*, pages 8818–8827, 2020.
- [20] Junhwa Hur and Stefan Roth. Joint optical flow and temporally consistent semantic segmentation. In *European Conference on Computer Vision Workshops (ECCVw)*, pages 163–177. Springer, 2016.
- [21] Eddy Ilg, Nikolaus Mayer, Tonmoy Saikia, Margret Keuper, Alexey Dosovitskiy, and Thomas Brox. FlowNet 2.0: Evolution of optical flow estimation with deep networks. In *IEEE/CVF Conference on Computer Vision and Pattern Recognition (CVPR)*, pages 2462–2470, 2017.
- [22] Samvit Jain, Xin Wang, and Joseph E Gonzalez. Accel: A corrective fusion network for efficient semantic segmentation on video. In *IEEE/CVF Conference on Computer Vision and Pattern Recognition (CVPR)*, pages 8866–8875, 2019.

- [23] Lingtong Kong, Chunhua Shen, and Jie Yang. FastFlowNet: A lightweight network for fast optical flow estimation. In *International Conference on Robotics and Automation (ICRA)*, pages 10310–10316. IEEE, 2021.
- [24] Abhijit Kundu, Xiaoqi Yin, Alireza Fathi, David Ross, Brian Brewington, Thomas Funkhouser, and Caroline Pantofaru. Virtual multi-view fusion for 3D semantic segmentation. In *European Conference on Computer Vision (ECCV)*, pages 518–535, 2020.
- [25] Yevhen Kuznietsov, Marc Proesmans, and Luc Van Gool. Towards unsupervised online domain adaptation for semantic segmentation. In *IEEE/CVF Winter Conference on Applications of Computer Vision (WACV)*, pages 261–271, 2022.
- [26] Jiangwei Lao, Weixiang Hong, Xin Guo, Yingying Zhang, Jian Wang, Jingdong Chen, and Wei Chu. Simultaneously short-and long-term temporal modeling for semi-supervised video semantic segmentation. In *IEEE/CVF Conference on Computer Vision and Pattern Recognition (CVPR)*, pages 14763–14772, 2023.
- [27] Seokju Lee, Sunghoon Im, Stephen Lin, and In So Kweon. Learning monocular depth in dynamic scenes via instance-aware projection consistency. In *Conference on Artificial Intelligence (AAAI)*, pages 1863–1872, 2021.
- [28] Jiangtong Li, Wentao Wang, Junjie Chen, Li Niu, Jianlou Si, Chen Qian, and Liqing Zhang. Video semantic segmentation via sparse temporal transformer. In *29th ACM International Conference on Multimedia (MM)*, pages 59–68, 2021.
- [29] Yifan Liu, Ke Chen, Chris Liu, Zengchang Qin, Zhenbo Luo, and Jingdong Wang. Structured knowledge distillation for semantic segmentation. In *IEEE/CVF Conference on Computer Vision and Pattern Recognition (CVPR)*, pages 2604–2613, 2019.
- [30] Yifan Liu, Chunhua Shen, Changqian Yu, and Jingdong Wang. Efficient semantic video segmentation with per-frame inference. In *European Conference on Computer Vision (ECCV)*, pages 352–368, 2020.
- [31] Lingni Ma, Jörg Stückler, Christian Kerl, and Daniel Cremers. Multi-view deep learning for consistent semantic mapping with RGB-D cameras. In *IEEE/RSJ International Conference on Intelligent Robots and Systems (IROS)*, pages 598–605, 2017.
- [32] Jelena Novosel, Prashanth Viswanath, and Bruno Arsenali. Boosting semantic segmentation with multi-task self-supervised learning for autonomous driving applications. In *NeurIPS-Workshops*, volume 3, 2019.
- [33] Adam Paszke, Sam Gross, Soumith Chintala, Gregory Chanan, Edward Yang, Zachary DeVito, Zeming Lin, Alban Desmaison, Luca Antiga, and Adam Lerer. Automatic differentiation in PyTorch. In *International Conference on Neural Information Processing Systems Workshops (NeurIPS-W)*, 2017.
- [34] Andra Petrovai and Sergiu Nedeveschi. Monodvps: A self-supervised monocular depth estimation approach to depth-aware video panoptic segmentation. In *IEEE/CVF Winter Conference on Applications of Computer Vision (WACV)*, pages 3077–3086, 2023.
- [35] Andreas Pfeuffer and Klaus Dietmayer. Separable convolutional lstms for faster video segmentation. In *IEEE Intelligent Transportation Systems Conference (ITSC)*, pages 1072–1078, 2019.
- [36] Andreas Pfeuffer, Karina Schulz, and Klaus Dietmayer. Semantic segmentation of video sequences with convolutional lstms. In *IEEE Intelligent Vehicles Symposium (IV)*, pages 1441–1447, 2019.

- [37] Siyuan Qiao, Yukun Zhu, Hartwig Adam, Alan Yuille, and Liang-Chieh Chen. ViP-DeepLab: Learning visual perception with depth-aware video panoptic segmentation. In *IEEE/CVF Conference on Computer Vision and Pattern Recognition (CVPR)*, pages 3997–4008, 2021.
- [38] Radu Alexandru Rosu, Jan Quenzel, and Sven Behnke. Semi-supervised semantic mapping through label propagation with semantic texture meshes. *International Journal of Computer Vision (IJCV)*, 128(5):1220–1238, 2020.
- [39] Daniel Seichter, Mona Köhler, Benjamin Lewandowski, Tim Wengefeld, and Horst-Michael Gross. Efficient RGB-D semantic segmentation for indoor scene analysis. In *IEEE International Conference on Robotics and Automation (ICRA)*, pages 13525–13531, 2021.
- [40] Evan Shelhamer, Kate Rakelly, Judy Hoffman, and Trevor Darrell. Clockwork convnets for video semantic segmentation. In *European Conference on Computer Vision Workshops (ECCVw)*, pages 852–868, 2016.
- [41] Hanyu Shi, Guosheng Lin, Hao Wang, Tzu-Yi Hung, and Zhenhua Wang. SpSequenceNet: Semantic segmentation network on 4D point clouds. In *IEEE/CVF Conference on Computer Vision and Pattern Recognition (CVPR)*, pages 4574–4583, 2020.
- [42] Mennatullah Siam, Sepehr Valipour, Martin Jagersand, and Nilanjan Ray. Convolutional gated recurrent networks for video segmentation. In *IEEE International Conference on Image Processing (ICIP)*, pages 3090–3094, 2017.
- [43] Mennatullah Siam, Mostafa Gamal, Moemen Abdel-Razek, Senthil Yogamani, Martin Jagersand, and Hong Zhang. A comparative study of real-time semantic segmentation for autonomous driving. In *IEEE Conference on Computer Vision and Pattern Recognition Workshops (CVPRw)*, pages 587–597, 2018.
- [44] Guolei Sun, Yun Liu, Hao Tang, Ajad Chhatkuli, Le Zhang, and Luc Van Gool. Mining relations among cross-frame affinities for video semantic segmentation. In *European Conference on Computer Vision (ECCV)*, pages 522–539, 2022.
- [45] Guolei Sun, Yun Liu, Henghui Ding, Min Wu, and Luc Van Gool. Learning local and global temporal contexts for video semantic segmentation. *IEEE Transactions on Pattern Analysis and Machine Intelligence (TPAMI)*, 2024.
- [46] Zachary Teed and Jia Deng. Raft: Recurrent all-pairs field transforms for optical flow. In *European Conference on Computer Vision (ECCV)*, pages 402–419, 2020.
- [47] Serin Varghese, Sharat Gujamagadi, Marvin Klingner, Nikhil Kapoor, Andreas Bar, Jan David Schneider, Kira Maag, Peter Schlicht, Fabian Huger, and Tim Fingscheidt. An unsupervised temporal consistency (TC) loss to improve the performance of semantic segmentation networks. In *IEEE/CVF Conference on Computer Vision and Pattern Recognition Workshops (CVPRw)*, pages 12–20, 2021.
- [48] Angel Villar-Corrales, Ani Karapetyan, Andreas Boltres, and Sven Behnke. MSPred: Video prediction at multiple spatio-temporal scales with hierarchical recurrent networks. In *British Machine Vision Conference (BMVC)*, 2022.
- [49] Jörg Wagner, Volker Fischer, Michael Herman, and Sven Behnke. Functionally modular and interpretable temporal filtering for robust segmentation. In *British Machine Vision Conference (BMVC)*, page 282, 2018.
- [50] Chaoyang Wang, José Miguel Buenaposada, Rui Zhu, and Simon Lucey. Learning depth from monocular videos using direct methods. In *IEEE/CVF Conference on Computer Vision and Pattern Recognition (CVPR)*, pages 2022–2030, 2018.

- [51] Hao Wang, Weining Wang, and Jing Liu. Temporal memory attention for video semantic segmentation. In *IEEE International Conference on Image Processing (ICIP)*, pages 2254–2258, 2021.
- [52] Jingdong Wang, Ke Sun, Tianheng Cheng, Borui Jiang, Chaorui Deng, Yang Zhao, Dong Liu, Yadong Mu, Mingkui Tan, Xinggang Wang, et al. Deep high-resolution representation learning for visual recognition. *IEEE Transactions on Pattern Analysis and Machine Intelligence (TPAMI)*, 2020.
- [53] Qin Wang, Dengxin Dai, Lukas Hoyer, Luc Van Gool, and Olga Fink. Domain adaptive semantic segmentation with self-supervised depth estimation. In *IEEE/CVF International Conference on Computer Vision (CVPR)*, pages 8515–8525, 2021.
- [54] Yu-Syuan Xu, Tsu-Jui Fu, Hsuan-Kung Yang, and Chun-Yi Lee. Dynamic video segmentation network. In *IEEE/CVF Conference on Computer Vision and Pattern Recognition (CVPR)*, pages 6556–6565, 2018.
- [55] Haobo Yuan, Xiangtai Li, Yibo Yang, Guangliang Cheng, Jing Zhang, Yunhai Tong, Lefei Zhang, and Dacheng Tao. Polyphonicformer: Unified query learning for depth-aware video panoptic segmentation. In *European Conference on Computer Vision (ECCV)*, pages 582–599. Springer, 2022.
- [56] Pierluigi Zama Ramirez, Matteo Poggi, Fabio Tosi, Stefano Mattoccia, and Luigi Di Stefano. Geometry meets semantics for semi-supervised monocular depth estimation. In *14th Asian Conference on Computer Vision (ACCV)*, pages 298–313. Springer, 2019.
- [57] Yizhe Zhang, Shubhankar Borse, Hong Cai, and Fatih Porikli. AuxAdapt: Stable and efficient test-time adaptation for temporally consistent video semantic segmentation. In *IEEE/CVF Winter Conference on Applications of Computer Vision (WACV)*, pages 2339–2348, 2022.
- [58] Yizhe Zhang, Shubhankar Borse, Hong Cai, Ying Wang, Ning Bi, Xiaoyun Jiang, and Fatih Porikli. Perceptual consistency in video segmentation. In *IEEE/CVF Winter Conference on Applications of Computer Vision (WACV)*, pages 2564–2573, 2022.
- [59] Hengshuang Zhao, Jianping Shi, Xiaojuan Qi, Xiaogang Wang, and Jiaya Jia. Pyramid scene parsing network. In *IEEE Conference on Computer Vision and Pattern Recognition (CVPR)*, pages 2881–2890, 2017.
- [60] Tianfei Zhou, Fatih Porikli, David J Crandall, Luc Van Gool, and Wenguan Wang. A survey on deep learning technique for video segmentation. *IEEE Transactions on Pattern Analysis and Machine Intelligence (TPAMI)*, 45(6):7099–7122, 2022.
- [61] Tinghui Zhou, Matthew Brown, Noah Snavely, and David G Lowe. Unsupervised learning of depth and ego-motion from video. In *IEEE/CVF Conference on Computer Vision and Pattern Recognition (CVPR)*, pages 1851–1858, 2017.
- [62] Minghan Zhu, Shizhong Han, Hong Cai, Shubhankar Borse, Maani Ghaffari, and Fatih Porikli. 4D panoptic segmentation as invariant and equivariant field prediction. In *IEEE/CVF International Conference on Computer Vision (ICCV)*, pages 22488–22498, 2023.
- [63] Xizhou Zhu, Yuwen Xiong, Jifeng Dai, Lu Yuan, and Yichen Wei. Deep feature flow for video recognition. In *IEEE/CVF Conference on Computer Vision and Pattern Recognition (CVPR)*, pages 2349–2358, 2017.

## A Evaluation Metrics

To evaluate MCDS-VSS, we compute its segmentation performance, temporal consistency, throughput and inference speed.

Following the standard practice, we use the mean Intersection over Union (mIoU) to evaluate the segmentation performance.

To evaluate the temporal consistency (TC) of a VSS model, we closely follow the procedure proposed by Liu *et al.* [30], in which we compute the mean flow warping error between every two neighboring frames. More precisely, we use FlowNet2 [21] to compute the optical flow between two adjacent frames, and warp the predicted segmentation maps from time-step  $t - 1$  into time  $t$ . We then calculate the mIoU between the warped and actual target segmentations. Following [30], we evaluate TC using a subset of 100 sequences from the validation set.

We measure the throughput and inference speed of our model in frames per second (FPS) and milliseconds (ms), respectively. For this purpose, we perform inference with MCDS-VSS on 200 different video sequences of 6 frames and average the throughput and time across frames and sequences.

## B Implementation Details

### B.1 Network Details

In this section, we describe the network architectures and operation of each module in MCDS-VSS. We emphasize that MCDS-VSS is architecture-agnostic and could be implemented with different, e.g. more powerful or efficient, model designs.

**Image Encoder & Segmentation Decoder:** We implement two distinct MCDS-VSS variants, whose image encoder and segmentation decoder follow the architecture of two popular image semantic segmentation models, namely DeepLabV3+ [6] with a ResNet18 [16] backbone and HRNetV2 [52] with a channel multiplier of 18, respectively. In both cases we initialize the parameters of the encoders with those of the model pretrained on ImageNet, whereas the segmentation decoders are initialized with random weights.

**Motion Encoder:** The motion encoder concatenates the image features from two consecutive time steps (i.e.  $\mathbf{h}_{t-1}$  and  $\mathbf{h}_t$ ) across the channel dimension, and processes this representation with three convolutional layers, followed by batch normalization and ReLU activation functions.

**Depth Decoder:** The network architecture of our depth decoder, which is reported in Table 5, closely follows [12, 13]. It is composed of five convolutional blocks using reflection padding, followed by ELU nonlinearities. Each of the last three convolutional blocks up-samples the feature maps by a factor of two using nearest-neighbor upsampling. The depth decoder outputs normalized inverse depth maps  $\mathbf{d}^s$ , which are then converted into depth maps  $\mathbf{d}$  by:

$$\frac{1}{\mathbf{d}} = \frac{1}{D_{\min}} + \left( \frac{1}{D_{\max}} - \frac{1}{D_{\min}} \right) \cdot \mathbf{d}^s, \quad (11)$$

where  $D_{\min}$  and  $D_{\max}$  are constant values defining the minimum and maximum depth values in the scene, set to  $D_{\min} = 0.1\text{m}$  and  $D_{\max} = 100\text{m}$  for the Cityscapes dataset.

**Ego-Motion Decoder:** The ego-motion decoder, which is reported in Table 6, processes the motion features with a series of convolution layers, followed by batch normalization

Table 5: Network architecture of the depth decoder module.

Layer	Modules	Output Dim.
Block 1	Conv + ELU	$256 \times H/8 \times W/8$
	Conv + ELU	$256 \times H/8 \times W/8$
Block 2	Conv + ELU	$128 \times H/8 \times W/8$
	Conv + ELU	$128 \times H/8 \times W/8$
Block 3	Conv + ELU + Ups.	$64 \times H/4 \times W/4$
	Conv + ELU	$64 \times H/4 \times W/4$
Block 4	Conv + ELU + Ups.	$32 \times H/2 \times W/2$
	Conv + ELU	$32 \times H/2 \times W/2$
Block 5	Conv + ELU + Ups.	$16 \times H \times W$
	Conv + ELU	$16 \times H \times W$
Disp. Pred.	Conv + Sigmoid	$1 \times H \times W$

Table 6: Network architecture of the ego-motion decoder module.

Layer	Modules	Output Dim.
Block 1	Conv + BN + ReLU	$256 \times H/8 \times W/8$
Block 2	Conv + BN + ReLU	$256 \times H/8 \times W/8$
Block 3	Conv + BN + ReLU	$128 \times H/8 \times W/8$
Block 4	Conv + Pool + ReLU	$128 \times H/16 \times W/16$
Ego Motion	Conv Global Avg. Pool	$6 \times H/16 \times W/16$ 6

Table 7: Training stages and hyper-parameters.

Stage	Training Goal	Loss Function	LR	Batch	Train Time	# Imgs
1	Segmentation & SSL Geometry	$\mathcal{L}_{\text{Seg}} + \lambda_{\text{D}} \cdot \mathcal{L}_{\text{Depth}}$	$2 \cdot 10^{-4}$	12	40h	3
2	Distillation of Object Motion	$\mathcal{L}_{\text{Flow}}$	$1 \cdot 10^{-4}$	4	18h	2
3	Ego-Motion Filter	$\mathcal{L}_{\text{Ego}}$	$8 \cdot 10^{-5}$	8	8h	6
4	Temporal Integration	$\mathcal{L}_{\text{Seg}} + \lambda_{\text{TC}} \cdot \mathcal{L}_{\text{TC}}$	$8 \cdot 10^{-5}$	4	12h	6

and ReLU nonlinearities. The final layer outputs a 6-dimensional vector representing the translation and rotation (parameterized as Euler angles) of the camera transformation matrix.

**Residual Flow Decoder:** The residual flow decoder is implemented as a modified lightweight version of RAFT [46]. To seamlessly integrate this module into our MCDS-VSS filter, we modify the implementation of `raft_small` provided by PyTorch<sup>2</sup> by replacing the expensive feature and context encoders with a single convolutional block that directly processes the ego-warped  $\mathbf{s}_t^{\text{ego}}$  and image features  $\mathbf{h}_t$ . We set the number of refinement iterations to 10.

**MCDS-VSS Filter:** We instantiate the MCDS-VSS filter using the modules described above, after being pretrained for semantic segmentation, SSL of depth and ego-motion, and distillation of object motion. For the first image in a video sequence, MCDS-VSS directly predicts its semantic segmentation, without the use of any temporal filtering. For all other frames, MCDS-VSS employs the structured filtering method described in the paper. The scene feature state is initialized with the image features from the first frame in the video sequence ( $\mathbf{s}_1 = \mathbf{h}_1$ ), whereas the initial camera state  $\mathbf{c}_1$  is initialized with zeros. We experimented with learning the initial state representations; however it did not yield any qualitative or quantitative improvements, while increasing the number of learnable parameters.

## B.2 Training and Inference

All our models are implemented in PyTorch [53] and trained with two NVIDIA A100 (80GB) GPUs. For each of the four training stages undergone by MCDS-VSS, we report in Table 7 the most relevant hyper-parameters, including the approximate training time, learning rate,

<sup>2</sup><https://pytorch.org/vision/main/models/raft.html>

Table 8: Throughput, inference speed (in ms) and number of learnable parameters for MCDS-VSS based on DeepLabV3+.

Model	# Params.	FPS	Inf. (ms)
Image Enc $\mathcal{E}_x$	15.3M	76.9	12.9
Motion Enc $\mathcal{E}_m$	4.8M	279.4	3.6
Motion Update	2.8M	476.2	2.1
Ego-Motion Dec $\mathcal{D}_c$	1.6M	492.8	2.0
Depth Dec $\mathcal{D}_d$	1.9M	227.1	4.4
Ego-Motion Comp.	0	63.4	15.8
Residual Flow Dec $\mathcal{R}_f$	2.7M	14.0	71.8
Object Motion Comp.	0	775.6	1.3
Feature Fusion	2.6M	215.3	4.6
Segmentation Dec $\mathcal{D}_y$	1.3M	196.7	5.1
Total MCDS-VSS	32.9M	9.0	111.6

Table 9: Throughput, inference speed (in ms) and number of learnable parameters for MCDS-VSS based on HRNetV2.

Model	# Params.	FPS	Inf. (ms)
Image Enc $\mathcal{E}_x$	9.5M	36.7	27.2
Motion Enc $\mathcal{E}_m$	5.0M	75.8	13.2
Motion Update	2.8M	166.7	6.0
Ego-Motion Dec $\mathcal{D}_c$	1.6M	174.4	5.7
Depth Dec $\mathcal{D}_d$	1.9M	62.4	16.0
Ego-Motion Comp.	0	47.9	20.9
Residual Flow Dec $\mathcal{R}_f$	2.9M	13.4	74.6
Object Motion Comp.	0	886.2	1.1
Feature Fusion	2.6M	76.8	13.0
Segmentation Dec $\mathcal{D}_y$	78.8K	627.6	1.6
Total MCDS-VSS	26.2M	5.6	177.6

batch size and number of images per sequence. We empirically set the loss weight values to  $\lambda_D = 2$ ,  $\lambda_{\text{Reg}} = 10^{-5}$  and  $\lambda_{\text{TC}} = 1$ .

Tables 8 and 9 report the number of learnable parameters, throughput and inference time for each individual module, as well as for the complete model, for the MCDS-VSS variants based on DeepLabV3+ and HRNetV2, respectively. We emphasize that the ego-motion and object motion compensation modules do not have any learnable parameters, but instead hardwire our knowledge from the moving camera dynamic scene domain to project the previous scene features into the current time-step using geometry and motion representations. We also observe that MCDS-VSS inference is severely limited by its residual flow decoder. Adapting such module to exploit recent advances in fast optical flow estimation [23], as well as using more efficient image encoders [17], could allow MCDS-VSS to be used for real time video semantic segmentation.

## C Additional Quantitative Results

In Table 10 we compare for individual classes of the Cityscapes dataset the segmentation performance and temporal consistency of MCDS-VSS with an HRNetV2 baseline trained for semantic segmentation and SSL of geometry and motion. MCDS-VSS achieves the best segmentation performance and temporal consistency for most classes in the dataset, especially for those corresponding to moving objects, such as *car*, *truck*, *bus* or *train*.

## D Additional Qualitative Results

### D.1 Effect of Each MCDS-VSS Stage

In Fig. 4 we display the semantic segmentations obtained when decoding the scene features from different stages of our MCDS-VSS filter. We can observe how the segmentations after ego-motion compensation (Fig. 4 b) atone for the movement of the ego-vehicle, correctly representing static scene features such as buildings or the bicycle. However, the dynamics of moving objects (e.g. yellow car) are not addressed in this step, thus not compensating for such movement. This limitation is addressed in the object motion compensation step

Table 10: Segmentation performance (mIoU) and temporal consistency (TC) for individual Cityscapes classes. We compare MCDS-VSS with HRNetV2 backbone with an HRNetV2 model trained for semantic segmentation and SSL of geometry and motion.

		<i>Road</i>	<i>Sidewalk</i>	<i>Building</i>	<i>Wall</i>	<i>Fence</i>	<i>Pole</i>	<i>Traf. Light</i>	<i>Traf. Sign</i>	<i>Person</i>	<i>Rider</i>	<i>Car</i>	<i>Truck</i>	<i>Bus</i>	<i>Train</i>	<i>Motorbike</i>	<i>Bicycle</i>	<i>Mean</i>
mIoU	Baseline	<b>98.1</b>	84.3	92.5	50.3	59.2	<b>66.5</b>	70.3	<b>79.3</b>	<b>81.8</b>	63.5	94.6	72.4	83.5	67.7	61.4	76.6	76.5
	Ours	<b>98.1</b>	<b>84.7</b>	<b>92.7</b>	<b>51.3</b>	<b>59.6</b>	65.9	<b>70.5</b>	<b>79.3</b>	81.6	<b>63.7</b>	<b>94.9</b>	<b>77.6</b>	<b>85.0</b>	<b>70.6</b>	<b>61.7</b>	<b>76.7</b>	<b>77.1</b>
TC	Baseline	98.7	86.0	91.1	60.8	60.1	67.1	62.4	77.1	69.0	65.8	89.0	58.1	66.8	45.8	49.4	66.6	71.7
	Ours	<b>98.9</b>	<b>88.2</b>	<b>92.1</b>	<b>64.1</b>	<b>65.9</b>	<b>69.1</b>	<b>69.2</b>	<b>79.5</b>	<b>70.5</b>	<b>67.8</b>	<b>90.5</b>	<b>65.2</b>	<b>69.6</b>	<b>48.3</b>	<b>53.6</b>	<b>71.0</b>	<b>75.3</b>

(Fig. 4 c). However, the disocclusions resulting from the moving car and inaccuracies in the residual flow estimation can lead to segmentation errors. Finally, fusing the projected scene state features with the current observations (Fig. 4 d) leads to a more accurate segmentation of the scene. In (Fig. 4 e) we visualize the update gate mask  $\mathbf{u}$  employed for feature fusion. For visualization purposes, we take the mean across all channels and assign lighter colors to spatial locations where MCDS-VSS relies on the propagated state  $\mathbf{s}_t^{\text{full}}$ , whereas darker colors correspond to the current features  $\mathbf{h}_t$ . We observe that MCDS-VSS relies on the scene state to represent static areas such as buildings or the street, whereas it relies heavier on observations for accurately segmenting fast moving objects or thin structures (e.g. poles or street signs).

## D.2 MCDS-VSS Qualitative Results

Despite being trained without any depth or motion labels, and solely with semantic segmentation annotations for a single frame per video, our model parses the scene into semantic, geometry and motion representations. In Figs. 5–8, we show on four validation sequences how MCDS-VSS obtains an accurate and temporally consistent segmentation of the scene, estimates the scene depth, and computes the residual motion flow, which encodes the movement of dynamic objects in the scene, as well as some minor motion corrections for other objects and scene features.

## D.3 Point Clouds

Figs. 9–12 show examples of RGB and semantic point clouds rendered by backprojecting image values and semantic labels using the depth maps estimated by MCDS-VSS and known camera intrinsics. The high-quality depth maps computed by MCDS-VSS allow for an accurate 3D representation of the scene.

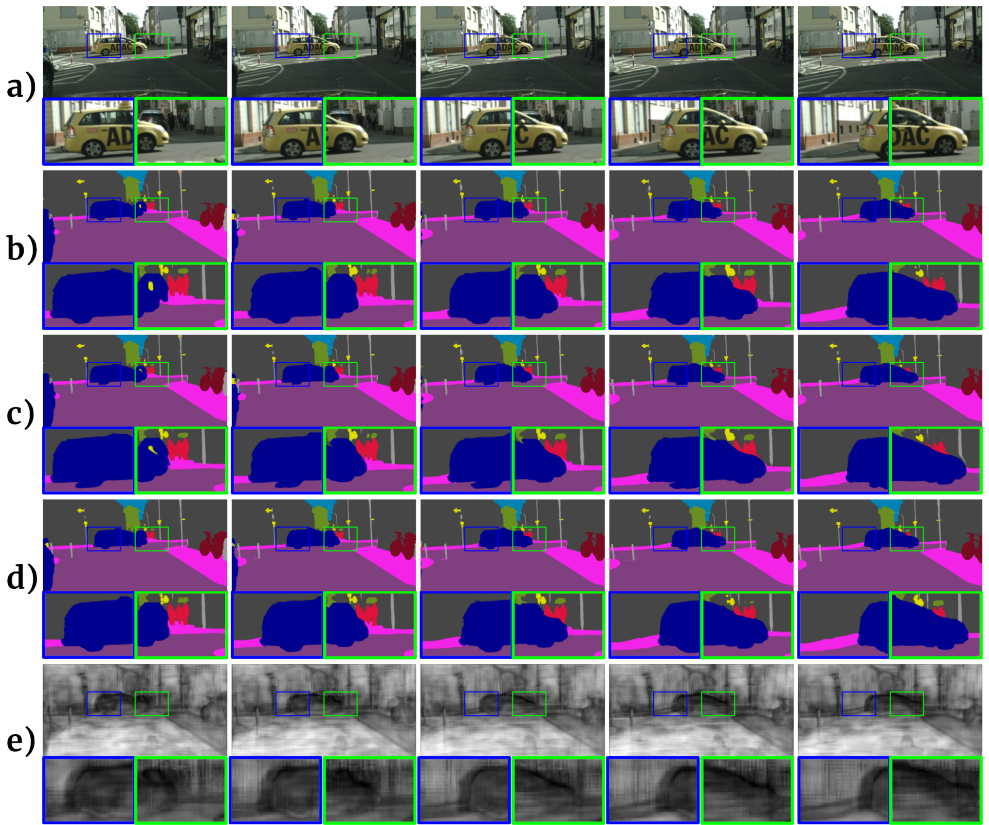


Figure 4: Video segmentation for each stage in MCDS-VSS. **a)** Input images, **b)** segmentation after ego-motion compensation, **c)** segmentation after object motion compensation, **d)** segmentation after feature fusion, **e)** feature fusion update mask, lighter colors mean that filter information is used, whereas darker ones correspond to observations.

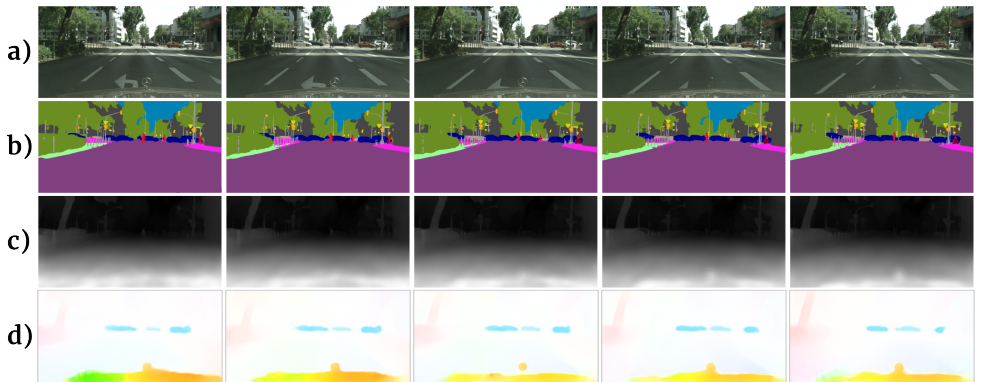


Figure 5: MCDS-VSS qualitative evaluation. **a)** Input frames, **b)** semantic segmentation, **c)** scene depth, **d)** residual flow.

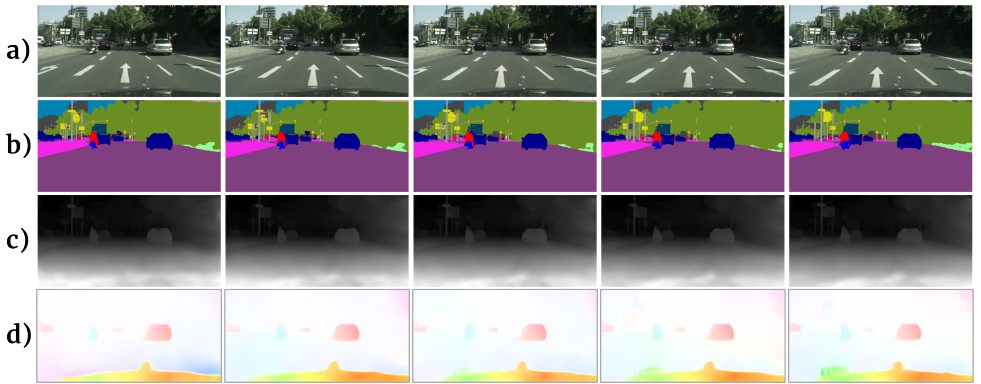


Figure 6: MCDS-VSS qualitative evaluation. **a)** Input frames, **b)** semantic segmentation, **c)** scene depth, **d)** residual flow.

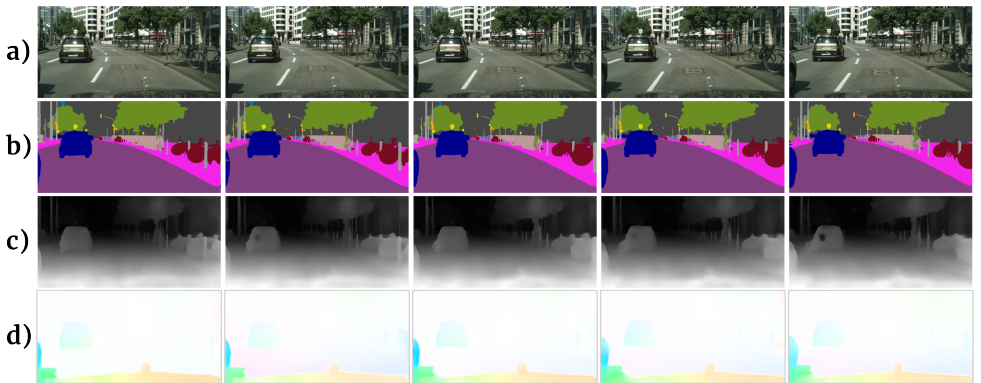


Figure 7: MCDS-VSS qualitative evaluation. **a)** Input frames, **b)** semantic segmentation, **c)** scene depth, **d)** residual flow.

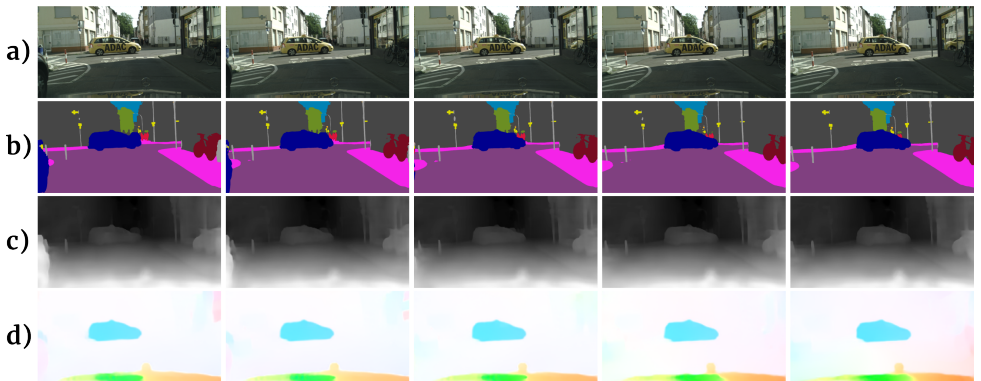


Figure 8: MCDS-VSS qualitative evaluation. **a)** Input frames, **b)** semantic segmentation, **c)** scene depth, **d)** residual flow.



Figure 9: RGB and semantic point clouds rendered by lifting image values and semantic labels to 3D space.

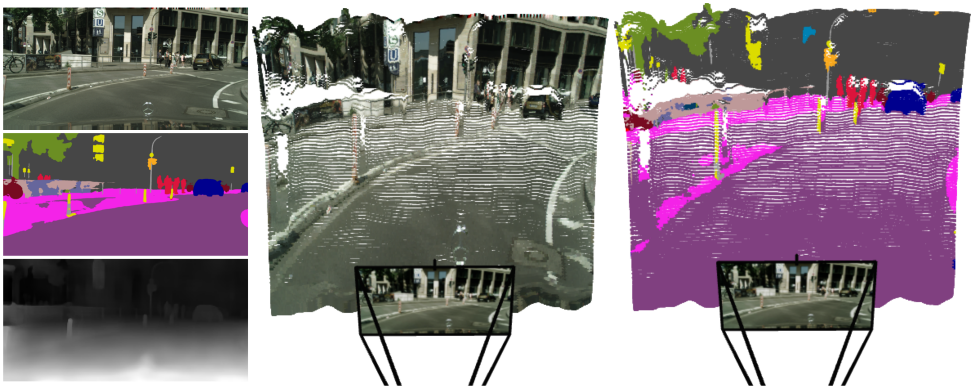


Figure 10: RGB and semantic point clouds rendered by lifting image values and semantic labels to 3D space.

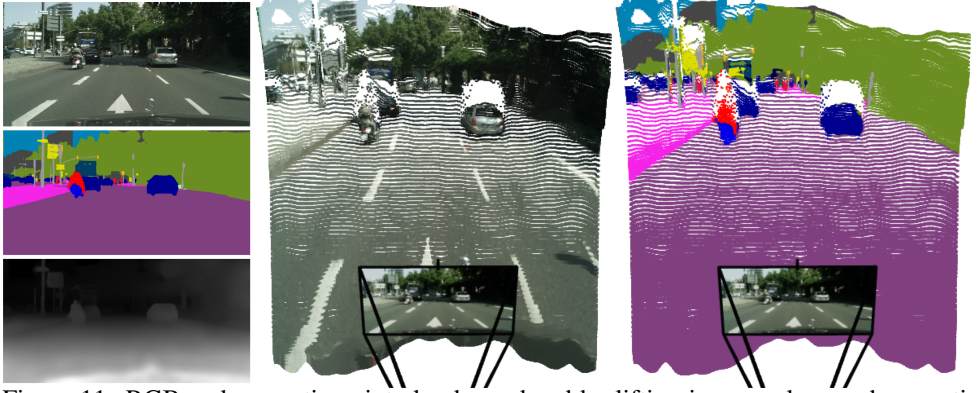


Figure 11: RGB and semantic point clouds rendered by lifting image values and semantic labels to 3D space.

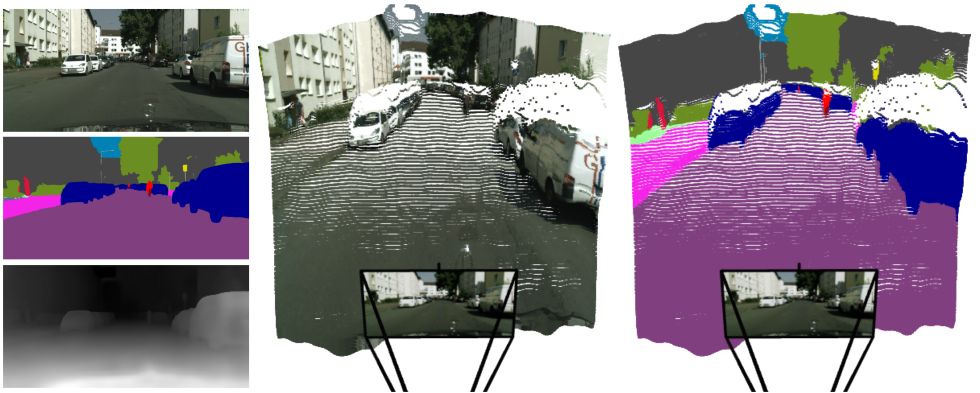


Figure 12: RGB and semantic point clouds rendered by lifting image values and semantic labels to 3D space.